Establishment of a bioluminescence model for microenvironmentally induced oral carcinogenesis with implications for screening bioengineered scaffolds

Salwa Suliman, BDS,[1,2,3] Himalaya Parajuli, BDS,[2,3] Yang Sun, PhD,[4] Anne Christine Johannessen, PhD,[2,5,6] Anna Finne–Wistrand, PhD,[4] Emmet McCormack, PhD,[7,8] Kamal Mustafa, PhD,[1] Daniela Elena Costea, PhD[2,5,6]*

[1]Department of Clinical Dentistry, Centre for Clinical Dental Research, University of Bergen, Bergen, Norway, [2]Gade Laboratory for Pathology, Department of Clinical Medicine, University of Bergen, Bergen, Norway, [3]Centre for International Health, Department of Global Public Health and Primary Care, University of Bergen, Bergen, Norway, [4]Department of Fibre and Polymer Technology, KTH Royal Institute of Technology, Stockholm, Sweden, [5]Centre for Cancer Biomarkers, Department of Clinical Medicine, University of Bergen, Bergen, Norway, [6]Department of Pathology, Haukeland University Hospital, Bergen, Norway, [7]Department of Clinical Science, University of Bergen, Bergen, Norway, [8]Department of Medicine, Haematology Section, Haukeland University Hospital, Bergen, Norway.

Accepted 3 July 2015
Published online 14 August 2015 in Wiley Online Library (wileyonlinelibrary.com). DOI 10.1002/hed.24187

ABSTRACT: *Background.* Microenvironmental cues play a major role in head and neck cancer. Biodegradable scaffolds used for bone regeneration might also act as stimulative cues for head and neck cancer. The purpose of this study was to establish an experimental model for precise and noninvasive evaluation of tumorigenic potential of microenvironmental cues in head and neck cancer.

Methods. Bioluminescence was chosen to image tumor formation. Early neoplastic oral keratinocyte (DOK) cells were luciferase-transduced (DOK^{Luc}), then tested in nonobese diabetic severe combined immunodeficient IL2rγnull mice either orthotopically (tongue) or subcutaneously for their potential as "screening sensors" for diverse microenvironmental cues.

Results. Tumors formed after inoculation of DOK^{Luc} were monitored easier by bioluminescence, and bioluminescence was more sensitive in detecting differences between various microenvironmental cues when compared to manual measurements. Development of tumors from DOK^{Luc} grown on scaffolds was also successfully monitored noninvasively by bioluminescence.

Conclusion. The model presented here is a noninvasive and sensitive model for monitoring the impact of various microenvironmental cues on head and neck cancer in vivo. © 2015 The Authors Head & Neck Published by Wiley Periodicals, Inc. *Head Neck* **38**: E1177–E1187, 2016

KEY WORDS: cancer, microenvironment, bioluminescence, tissue engineering, scaffold

INTRODUCTION

Recent evidence implicates environmental cues as key factors in cancer progression.[1] Among the important determinants is the surrounding stroma, including fibroblasts, endothelial cells, infiltrating immune cells, and extracellular matrix components.[2,3] The scaffolds used in tissue engineering as provisional matrices for cell proliferation and extracellular matrix deposition can also act as microenvironmental cues. The surrounding tissues might react toward these by foreign body reactions or even tumor formation,[4] and long-term subcutaneous implants of nonabsorbable or slowly degrading materials were shown to be tumorigenic.[5,6] Thus, there is a great concern that certain biomaterials may be potential initiators of malignancies, and the size and surface roughness of certain biomaterials were already suggested to influence tumor formation.[7] To date, at the regulatory level, the basic approach for biomaterials' safety is defined in the International Organization for Standardization 10993.[8,9] These tests start with an initial safety evaluation targeting leachable for cytotoxicity. Genotoxicity and evaluation of mRNA levels of proto-oncogenes and tumor suppressor genes[10] from mammalian or bacterial cells exposed to the biomaterials has also been used as methods for safety check.[11] Current carcinogenicity tests determine the tumorigenic potential of materials and/or their extracts from either single or multiple exposures or contacts over a period of the major portion of the life span of the test animal or transgenic mice.[12] Long-term, conventional 2-year rodent bioassays are often not feasible, with questionable relevance also because of limitations associated with species extrapolation.[13,14] Finding a relevant animal model for every kind of human cancer is impractical, but preclinical animal xenograft tumor models, particularly heterotopic (subcutaneous), have proven useful especially in identifying cytotoxic agents.[15–18] On the other hand, although more technically demanding, the orthotopic xenograft models simulate the same local microenvironment and thus offer the advantage of less complicated translation to the clinical setting.[19]

***Corresponding author:** D. E. Costea, Department of Clinical Medicine and Department of Clinical Dentistry, University of Bergen, 5009 Bergen, Norway. E-mail: daniela.costea@k1.uib.no

Contract grant sponsor: This work was funded by VascuBone project, EU FP7; no. 242175 and Bergen Medical Research Foundation (grant no. 20/2009), The Norwegian Cancer Research Association (grant no. 515970/2011), Norwegian Cancer Society (grant no. 732200), and Helse Vest (grant nos. 911902/2013, 911884, and 911789).

Scaffolds used for bone regeneration in the oral and maxillofacial area might come in contact with the oral epithelium. Because over 90% of head and neck cancers are, as most of the human malignancies, of epithelial origin,[20,21] there is a need to study the potentially carcinogenic effect of degradable bioengineered scaffolds on oral epithelial cells. To study oral and head and neck carcinogenesis, both orthotopic and heterotopic (subcutaneous) models were previously developed by use of malignant cells derived from established oral or head and neck cancer.[22] In this study, we chose to develop a xenotransplantation model by use of an early neoplastic oral keratinocyte (DOK) cell line derived from early neoplastic oral mucosa.[23] These cells were found to be partly transformed but nontumorigenic in nude mice, and were described as having potential as "screening recipients" for carcinogens in vitro.[23]

Different in vivo optical imaging modalities have been tested in various tumor models.[24–26] However, there is a need for a noninvasive head and neck cancer model with the ability to detect possible tumorigenic effects of various microenvironmental cues, including implanted scaffolds. Bioluminescent imaging is a well-established method in preclinical investigation of the complexity of cancers[27–29] including head and neck cancer,[30,31] but for a screening of the potential to fully transform and generate malignant tumors from the early neoplastic cells, the application of bioluminescence would offer a novel noninvasive approach. In carcinogenicity testing of biomaterials, controls of a comparable form and shape should be included. However, in the presented system, the use of appropriate controls is not necessary because the inclusion of a positive environment with the use of carcinoma-associated fibroblasts (CAFs) has been developed. The noninvasive in vivo visualization for several weeks also provides additional unique advantages over the aforementioned established carcinogenicity testing systems.

To achieve real-time bioluminescence in this study, DOK cells were first transduced to contain the firefly luciferase. They were then tested in vivo in NSG mice for their potential as "screening sensors" for diverse microenvironmental cues, such as various types of head and neck CAFs and copolymer scaffolds intended for tissue engineering. The biodegradable poly L-lactide-co-ε-caprolactone (poly[LLA-co-CL]), an aliphatic polyester copolymer of L-lactic acid and ε-caprolactone, has been extensively studied at our laboratory as a scaffold for bone regeneration proving its biocompatibility and osteo-conductivity,[8,32] and, hence, was chosen for developing this model.

MATERIALS AND METHODS

Cell choice and maintenance

The DOK cell line was purchased from The European Collection of Cell Cultures (Salisbury, Wiltshire, UK).[23] They were maintained in Dulbecco's modified Eagle's medium (DMEM) supplemented with 10% fetal calf serum (FCS; Invitrogen, Waltham, MA), 20 μg/mL L-glutamine, 5 μg/mL hydrocortisone (all from Sigma, St. Louis, MO).

CAFs ($n = 3$; CAF1, CAF15_13, and CAF15_23) were isolated from histologically confirmed head and neck squamous cell carcinoma, after receiving informed consent. They were maintained in FAD medium: DMEM/Ham's F12 1:3 mixture, 1% L-glutamine, 0.4 μg/mL hydrocortisone, 50 μg/mL ascorbic acid, 10 ng/mL epidermal growth factor, 5 μg/mL insulin, and 20 μg/mL transferrin and linoleic acid (all from Sigma) with 10% FCS.

Luciferase transduction of early neoplastic oral keratinocytes

Virus production. DOK wild type (DOK^{WT}) cells were transduced with a tTA, L192 construct (expressing luciferase).[33] Infectious retroviral vector particles were produced in Phoenix A cells (LGC Standards AB, Boras, Sweden) cultured in DMEM, supplemented with 10% FCS, 1% penicillin-streptomycin, and 1% glutamine. When 70% to 80% was confluent, 8 μL of 50 m*M* chloroquine (Sigma) was added. Four micrograms of DNA construct (tTA, L192) was mixed with 128 μL of 2M calcium chloride ($CaCl_2$) and sterile ddH_2O to a total volume of 1 mL plus 1 mL of 2×HEPES-buffered (Sigma) and transferred onto each plate. After 12-hour incubation, the medium was replaced by a fresh medium and by DOK's medium after 24 hours.

Infection and selection of luciferase-transduced early neoplastic oral keratinocyte. The virus supernatant was collected, filtered, and gene transfer enhanced with protamine sulfate (5 μg/mL). DOK^{WT} were seeded at 3 different seeding densities (25×10^3; 50×10^3; and 100×10^3 cells/well) in a 6-well plate and centrifuged at 1200 g for 90 minutes. The virus supernatant was replaced with the DOK medium 24 hours postinfection. Successfully infected DOK cells were selected by puromycin (1 μg/mL; Sigma). To obtain a cell-clone with a stable, high expression of luciferase, transduced DOK cells were sorted using fluorescence-activated cell sorter (FACS Aria SORP, BD Biosciences, San Jose, CA).

Selection of highly bioluminescent early neoplastic oral keratinocyte luciferase-transduced cells

Approximately 1×10^6 cells of each group in 100 μL DOK medium were transferred to 96-well plate with 1 well containing 100 μL of DOK medium only for background autofluorescence. Luciferin, (1.6 g/L of D-luciferin; Biosynth AG, Staad, Switzerland) was added 10 minutes before imaging in the Time-Domain Small Molecular Imager Optix MX3 (ART; GE Healthcare, Little Chalfont, UK). Using the OptiView acquisition software (ART Advanced Research Technologies, Quebec, Canada), the region of interest was chosen and plates were scanned with the scan step 1.0 mm and integration time 0.1 seconds.

Assessment of cell morphology and proliferation

Both cell types, DOK^{WT} and early neoplastic oral keratinocyte luciferase-transduced (DOK^{Luc}), were cultured at passages (45–48) and their morphology was compared under a light microscope (Nikon TS100; Nikon, Tokyo, Japan). The growth rate was analyzed using a colorimetric assay based on methylthiazol tetrazolium (Sigma) and measured at 570 nm using a microplate reader (BMG LABTECH, GmbH, Ortenberg, Germany).

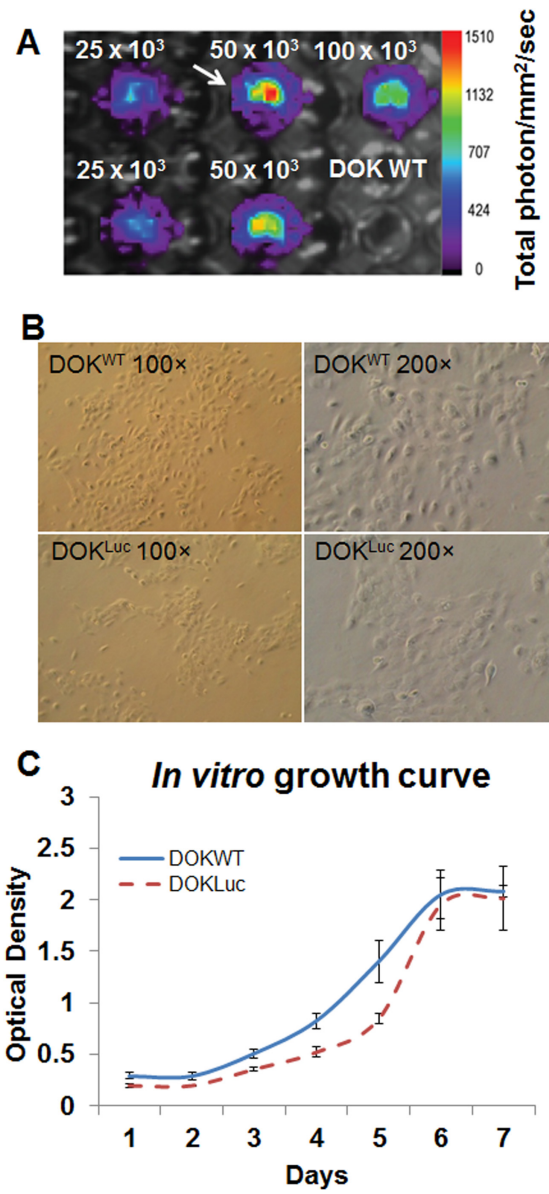

FIGURE 1. (A) Bioluminescence of early neoplastic oral keratinocyte luciferase-transduced (DOK^{Luc}) cells at a density of 50×10^3 early neoplastic oral keratinocyte wild type (DOK^{WT}) transduced 4 times, displaying the highest photons/mm²/sec, white arrow. (B) Light microscopy showing that DOK^{WT} and DOK^{Luc} exhibit the same typical morphology and pattern of growth in the form of coherent islands. (C) Growth curves for both cell types, showing no significant difference ($p = .262$) between the in vitro growth potential of DOK^{WT} and DOK^{Luc}.

Assessment of tumorigenicity in vivo

Both DOK^{WT} and DOK^{Luc} cells were cultured and allowed to reach their log phase before they were trypsinized and suspended in 50 μL of growth factor-reduced matrigel (BD Biosciences). The cells were inoculated at 2 different densities, low (1×10^3) and high (1×10^5), at 2 different locations, the tongue and subcutaneously in the back of 8 to 10 weeks old male nonobese diabetic severe combined immunodeficient IL2rγ^{null} mice (NSG) (University of Bergen - originally a generous gift from Prof. Leonard D. Shultz, Jackson Laboratories, Bar Harbor, ME; $n = 24$, 6 mice for each group). Weekly for 6 weeks, tumor volumes for both cell types were manually assessed by digital caliper, using the formula [length × (width²)/2]. In the group inoculated with DOK^{Luc}, tumor development was also measured weekly by bioluminescence. We euthanized the mice after 45 days and harvested tissues for histology.

Orthotopic tongue xenograft mouse model for early neoplastic oral keratinocyte + carcinoma-associated fibroblast co-inoculations

To create a positive tumor formation control, 1×10^3 DOK^{WT} were suspended with 1×10^5 CAFs (CAF1) in 50 μL matrigel and inoculated in the tongue of NSG mice ($n = 12$; 6 mice for each group). Tumors were measured manually up to 45 days.

To assess the sensitivity of bioluminescence to differentiate between tumors formed by different strains of CAFs, DOK^{Luc} in a density of 1×10^3 were co-inoculated in combination with 1×10^5 of 2 different strains of CAFs (CAF15_13 and CAF15_23) in the tongue. The total number of animals was 24 with at least 6 for each group. The development of the tumors in this group was followed up manually and evaluated weekly by bioluminescence.

Preparation of cell-seeded poly L-lactide-co-ε-caprolactone scaffolds for ectopic subcutaneous scaffold xenograft

The copolymer poly(LLA-co-CL) was polymerized from ε-caprolactone (Sigma–Aldrich, Germany) and LLA (Boehringer, Ingelheim, Germany) by ring-open-polymerization, as previously described.[32] The average molecular weight of the purified copolymer was 100,000 and polydispersity index 1.3 determined by Size Exclusion Chromatography (Polymer Laboratories, Shropshire, UK). The copolymer was composed of 75 mol % LLA and 25 mol % caprolactone, confirmed by ^{1}H-NMR (Bruker Avance 400, Billerica, MA). The porous scaffolds were prepared by solvent casting particulate leaching[32] and a disc-shaped scaffold (diameter approximately 6 mm, thickness approximately 1.3 mm) was formed with >83% porosities. Porosities were calculated by a Micro-CT (Sky Scan 1172 scanner, Kontich, Belgium) using 40 kV and 2.4 micron voxel and 3D analysis was carried using the software CT-Analyzer version 1.13 (Bruker).

The scaffolds were pre-wet with DOK medium and left for 2 to 3 hours before being then seeded with cells, DOK^{Luc} alone or DOK^{Luc} + CAFs (CAF1). Three different densities of DOK were used (1×10^3, 1×10^5, and 1×10^6); the density of CAFs was fixed to 1×10^5. Plates were vortexed (Eppendorf, Hamburg, Germany) and the cells were allowed to attach overnight before scaffolds were xenotransplanted in 8 to 10-week-old NSG mice.

The mice were anesthetized with Isoflurane (Isoba VetTM; Schering Plough, Kenilworth, NJ) before 2 incisions (1 cm) were made on their back. One incision was

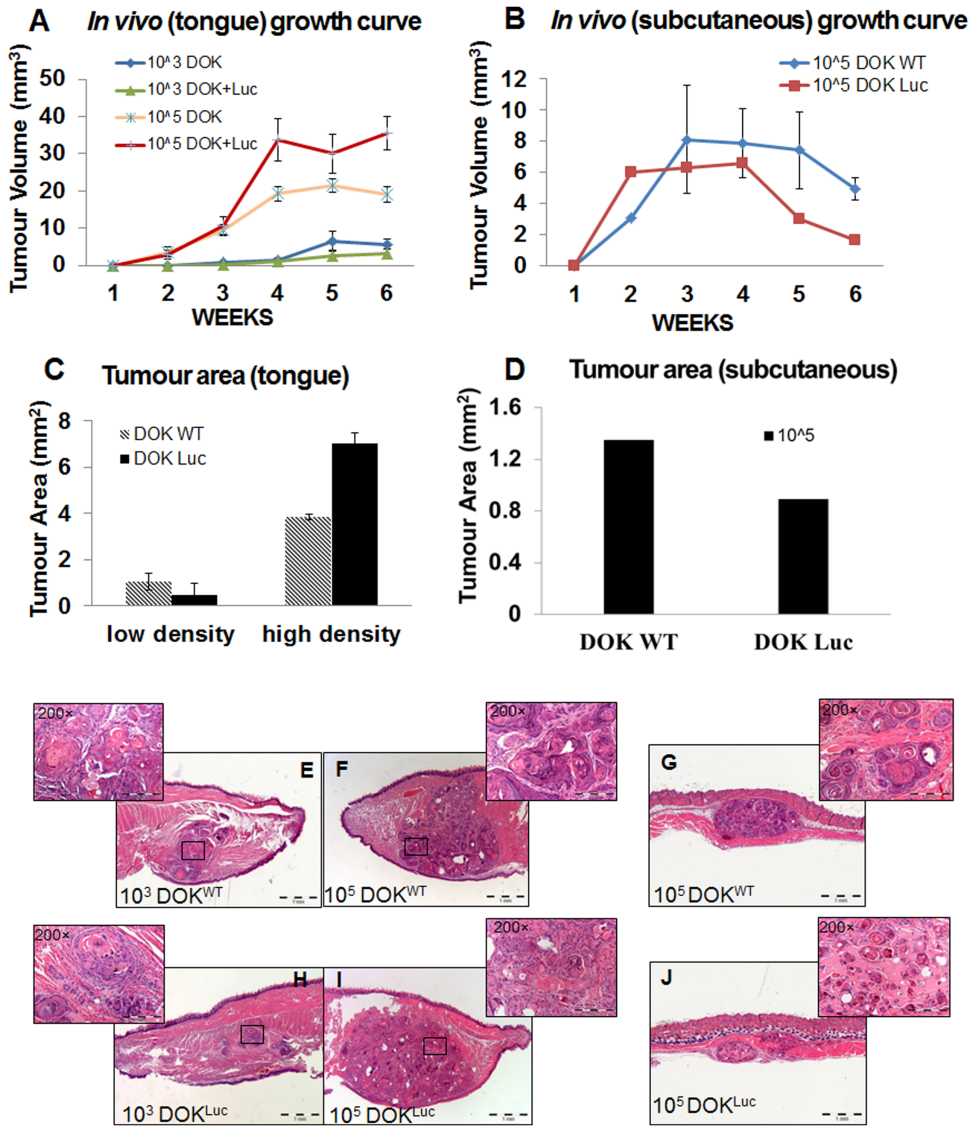

FIGURE 2. Graphs comparing the growth rate (tumor volume) and the total area of tumors formed by either early neoplastic oral keratinocyte wild type (DOK^{WT})or early neoplastic oral keratinocyte luciferase-transduced (DOK^{Luc}) inoculated at cell densities of 10^3 or 10^5 in the tongues (A and C), and subcutaneously (B and D) of NSG mice (*$p < .05$). Histological sections with hematoxylin-eosin stain showing 6 weeks after inoculation of the tongue (E, F, H, and I) and skin (G and J). The tumors retain the characteristics of squamous cell carcinoma (original magnification ×25 and ×200). Scale bar 1 mm = ×25 and 200 μm = ×200.

made between the upper limbs and another between the lower limbs, providing sufficient space for implantation of scaffolds and to avoid bioluminescence bleeding. Two scaffolds were implanted into each mouse, 1 scaffold with DOK^{Luc} alone and the other with DOK^{Luc} + CAFs. The different densities were distributed among all mice (n = 6). Wounds were closed with Histoacryl tissue adhesive (B. Braun Surgical AS, Melsungen, Germany). At 12 weeks, the animals were euthanized with CO_2 overdose and scaffolds processed for histology.

Optical bioluminescence imaging

Mice were depilated and scanned after intraperitoneal delivery of 150 mg/kg of D-luciferin. Animals were maintained under 1% gas anesthesia during scanning. Images were captured using In Vivo MS FX PRO (Carestream Health, Rochester, NY) and analyzed using Carestream MI SE version 5.0.6.20, 1 exposure of 90-second duration.

Histology and immunohistochemistry

Samples were fixed in 4% paraformaldehyde before embedding in paraffin. Sections of 3 to 4 μm were stained with hematoxylin-eosin (Sigma). For p53 immunostaining, paraffin sections were deparaffinized and rehydrated. Epitope retrieval was performed by heating the sections in citrate buffer pH 6.0 in a microwave. Endogenous enzyme activity and unspecific binding were blocked using peroxidase block (DAKO, Golstrup, Denmark) and 10% normal goat serum (DAKO) for 5 minutes and 30 minutes, respectively, at room temperature. As primary antibody, p53 with a monoclonal specific antibody (DO-7 clone, DAKO) 1:50 was incubated for 1 hour at room temperature. For negative controls, samples were treated with antibody diluents alone. The bound reaction was visualized using 3, 3′-diaminobenzidine tetra hydrochloride (DAB, DAKO). Double staining with vimentin (DAKO) 1:1000 was carried out using a double stain kit (Envision G|2 double stain system; DAKO), in accord with the manufacturer's instructions. Tumor areas were

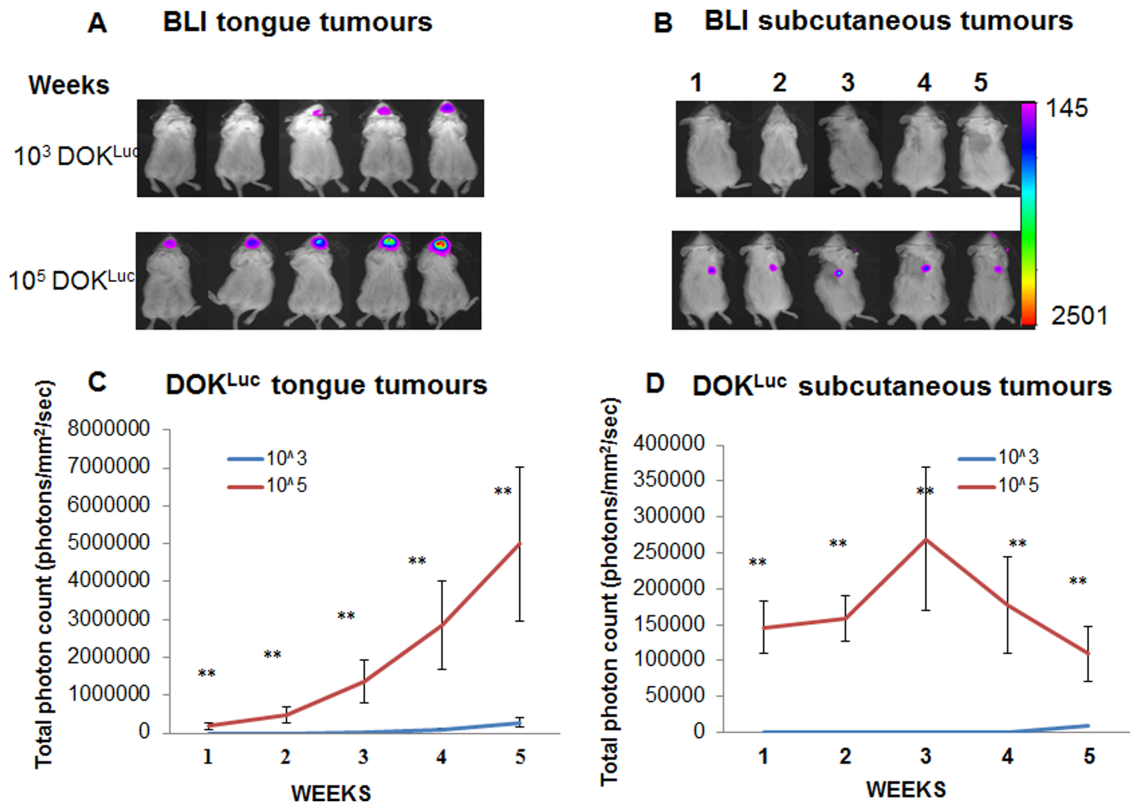

FIGURE 3. Bioluminescence (BLI) of mice for 5 weeks after inoculation with early neoplastic oral keratinocyte luciferase-transduced (DOK^{Luc}) cells (10^5 and 10^3 densities) in the tongue (A) and in the skin (B). Graphs depicting increasing total photon intensities from tongue inoculations (C) with a lower overall photon count produced from 10^3 densities (**$p < .01$). (D) Total photon intensities of cells for 5 weeks after subcutaneous inoculation (**$p < .01$). Data shown as means ± SEM.

calculated from areas of interest in hematoxylin-eosin sections using Olympus DP Soft 5.0 software (Munster, Germany).

Ethics statement

The ethical approval for patients with head and neck squamous cell carcinoma samples was obtained from the Regional Committees for Medical and Health Research Ethics (REK NO. 2010/48) and lesions were collected following ethical approval and written informed consent of the patients. All animal experiments were approved by the Norwegian Animal Research Authority and conducted in strict accordance with the European Convention for the Protection of Vertebrates used for Scientific Purposes (FOTS no. 20134643/20123961). All procedures were performed under isoflurane gas anesthesia, and all efforts were made to minimize suffering.

Statistical analysis

Average values were analyzed by IBM SPSS Statistics 21.0 (SPSS, Chicago, IL) and the data expressed as mean ± SEM. Paired *t* test or the independent Mann–Whitney *U* tests were used to compare differences between the tumors formed. Spearman's correlation was used to correlate the manual tumor measurements and histological measurements with corresponding bioluminescence signals. Differences were considered statistically significant when $p < .05$.

RESULTS

Successful transduction of early neoplastic oral keratinocyte with luciferase containing vector generated a new cell line

The bioluminescence signal recorded for DOK^{Luc} cells cultured in vitro for 2 to 3 weeks posttransduction showed that the seeding density of 50×10^3 displayed the highest photons/mm^2/sec (Figure 1A, white arrow). Cells derived following this protocol were expanded and used for further in vivo experiments. Light microscopy showed that DOK^{WT} and DOK^{Luc} had typical epithelial morphology and similar patterns of growth in the form of coherent islands. No signs of epithelial-to-mesenchymal transition could be observed in either (Figure 1B). The growth curve was comparable for the 2 cell types ($p = .262$), indicating that transduction with luciferase did not alter the in vitro growth potential of these cells (Figure 1C).

The in vivo tumorigenic potential of DOK cells before and after transduction with luciferase expressing gene was evaluated after DOK^{WT} and DOK^{Luc} were inoculated in the tongue and also subcutaneously in NSG mice at low (1×10^3) and high (1×10^5) density. At the high inoculation density, visible tumors were detected with the same incidence after 2 weeks, at both sites, for both DOK^{WT} and DOK^{Luc}. At the low density, tumors formed only in the tongue, and after 4 weeks, with the same incidence for

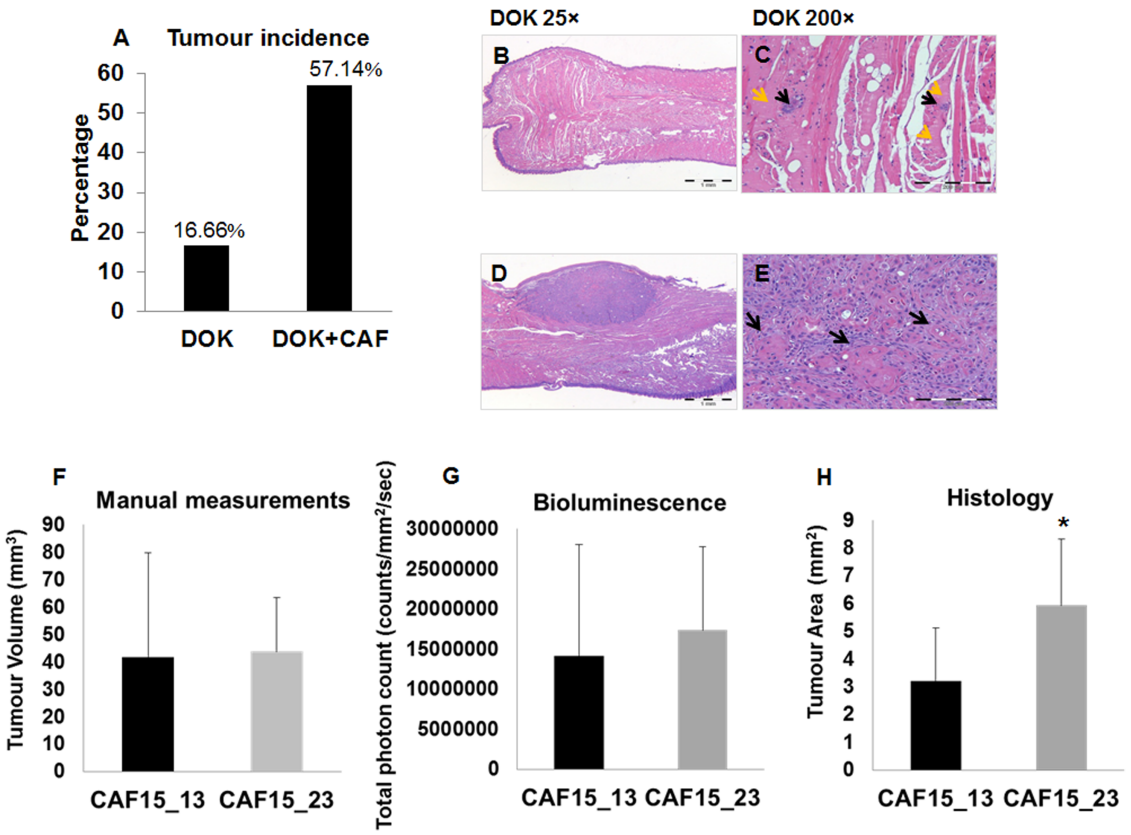

FIGURE 4. (A) Carcinoma-associated fibroblasts (CAFs) increased tumor incidence of early neoplastic oral keratinocytes wild type (DOK)^{WT} when co-inoculated in the tongues of NSG mice. (B and C) Hematoxylin-eosin section of the tumor detected in DOK^{WT} group presenting surviving DOK cells (black arrows) within remnants of matrigel (yellow arrows). (D and E) Hematoxylin-eosin section of tumor formed by DOK^{WT} + CAF; depicting typical squamous cell carcinoma morphology with keratin pearls (black arrows). (F) Graphs comparing the volumes by manual measurements from the last timepoint (week 7) of the tumors formed by 2 different strains of CAFs. (G) Comparison of total photon intensities at week 7 measured by bioluminescence. (H) Comparing tumor area from histology after 7 weeks (*$p = .028$).

DOK^{WT} and DOK^{Luc}. There was no statistical significance between the volume of the tumors formed in both tongue and subcutaneously by DOK^{WT} and DOK^{Luc} at all timepoints (Figures 2A and 2B). The histological area of the tumors derived from DOK^{WT} and DOK^{Luc} at low density in the tongue (Figure 2C) and at high density subcutaneously (Figure 2D) did not show any statistical significant difference. The only statistical significant difference was found for the tongue tumors formed at higher inoculation density by DOK^{Luc} than tumors formed by DOK^{WT} ($p < .05$; Figure 2C). Tumor xenografts generated from DOK^{WT} (Figures 2E–2G) showed the same histological picture as DOK^{Luc} xenografts (Figures 2H–2J), with epithelial islands of atypical epithelial cells in the host stroma and keratin pearls.

Development of tumors formed after inoculation of early neoplastic oral keratinocyte luciferase transduced cells was easily monitored by bioluminescence

Luciferase activity increased with time after both tongue and subcutaneous inoculations for both inoculation densities (Figures 3A and 3B). The bioluminescence signal was significantly higher for the inoculations of DOK^{Luc} at higher inoculation density at both tongue and subcutaneous locations (Figures 3C and 3D), at all timepoints, correlating well with the tumor growth curve as assessed by the manual measurements.

Both early neoplastic oral keratinocyte wild type and early neoplastic oral keratinocyte luciferase-transduced were responsive to carcinoma-associated fibroblast-derived microenvironmental cues and bioluminescence was more sensitive than manual measurement in detecting differences between various types of microenvironmental cues

Co-inoculating DOK^{WT} with 10^5 CAFs in the tongues of NSG mice increased tumor incidence from 16.66% to 57.14% (Figure 4A). Histological sections of the tumors formed by DOK^{WT} + CAF showed typical squamous cell carcinoma histology with invasive epithelial islands growing in the host stroma and keratin pearl formation (Figures 4D and 4E). The only 1 tumor formed by the DOK^{WT} alone, which was detected manually, was found histologically to be surviving DOK^{WT} cells within remnants of undissolved matrigel (Figures 4B and 4C). When 2 different types of fibroblasts (CAF15_13 and CAF15_23) were tested for their stimulative support for the in vivo growth of DOK^{Luc}, bioluminescence seemed to be more sensitive than the manual

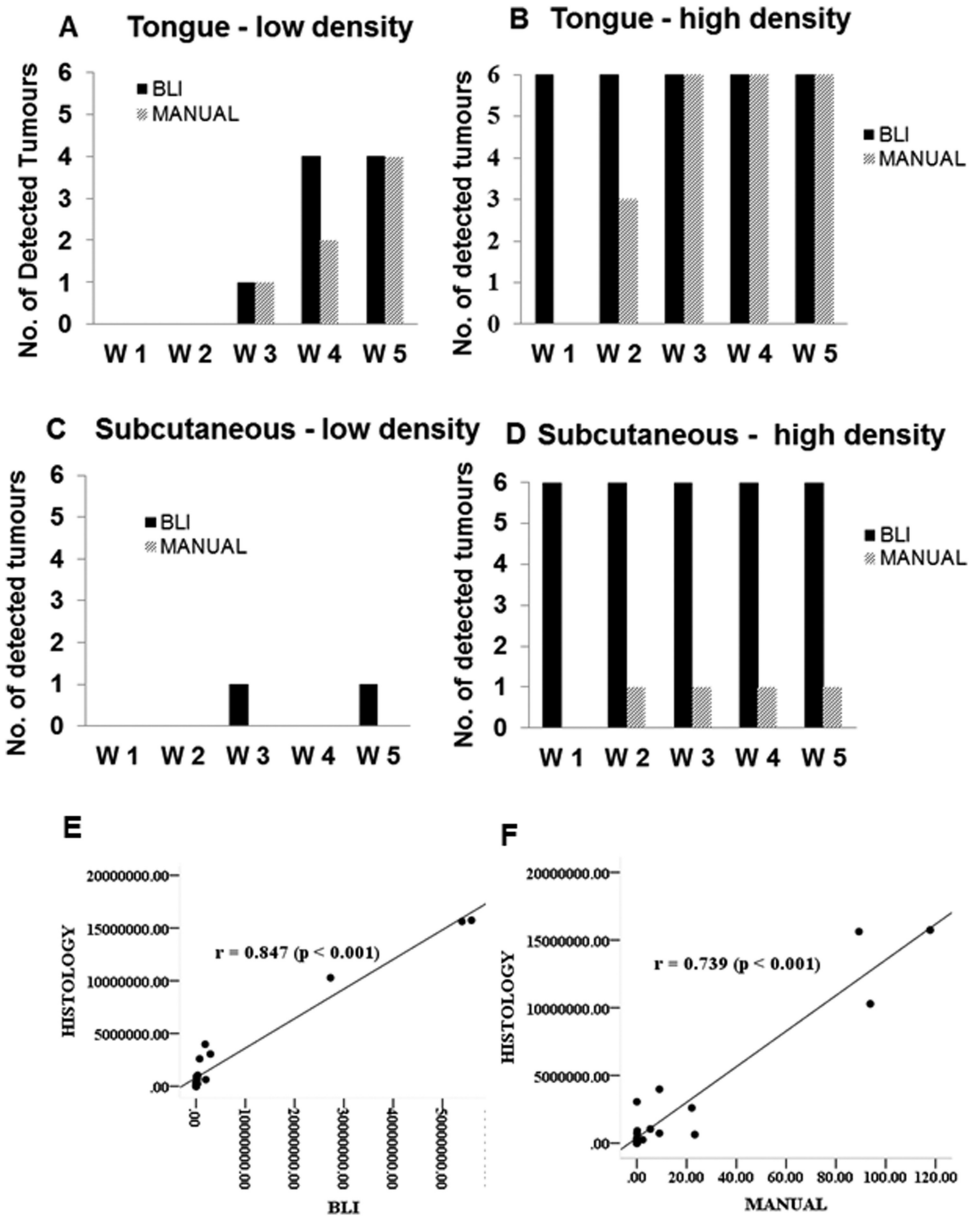

FIGURE 5. (A and B) Comparison of number of tumors detected by bioluminescence (BLI) and manually in the tongue inoculations at both densities. (C and D) Comparison in the skin inoculations ($p = .043$; $n = 24$). (E) Histological areas correlate with bioluminescence signals with a stronger correlation (Spearman's correlation, $r = 0.847$; $p < .001$); than with (F) manual measurements.

measurement in detecting differences in the tumor growth of xenografts (Figures 4F and 4G), although the difference was not statistically significant. This difference was also observed by histological area calculations after 7 weeks, this time with statistical significance ($p = .028$; Figure 4H).

Both bioluminescence and manual measurement showed high correlation with histological area of the tumors, but tumor formation was detected earlier by bioluminescence

Bioluminescence consistently disclosed a higher number of tumors throughout all 5 weeks of monitoring compared to visible tumors measured manually by calipers (Figures 5A–5D). Both the tumor volume as quantified by caliper (manual) measurements and the bioluminescence signal from the corresponding tumor at the last timepoint showed a positive correlation with the tumor area quantified from histological sections (considered to be the "golden standard"). A stronger significant correlation ($r = 0.846$; $p < .001$) was found between the histological tumor area and bioluminescence signals than between the histological tumor area and the manual measurement ($r = 0.739$; $p < .001$; Figures 5E and 5F).

Development of tumors from early neoplastic oral keratinocyte luciferase-transduced grown on poly L-lactide-co-ε-caprolactone scaffolds under different microenvironmental cues was successfully monitored noninvasively by bioluminescence

DOK^{Luc} were cultured on poly(LLA-co-CL) scaffolds at 3 different densities with or without CAFs. Total photon count from bioluminescence showed significantly higher bioluminescence intensity of scaffolds

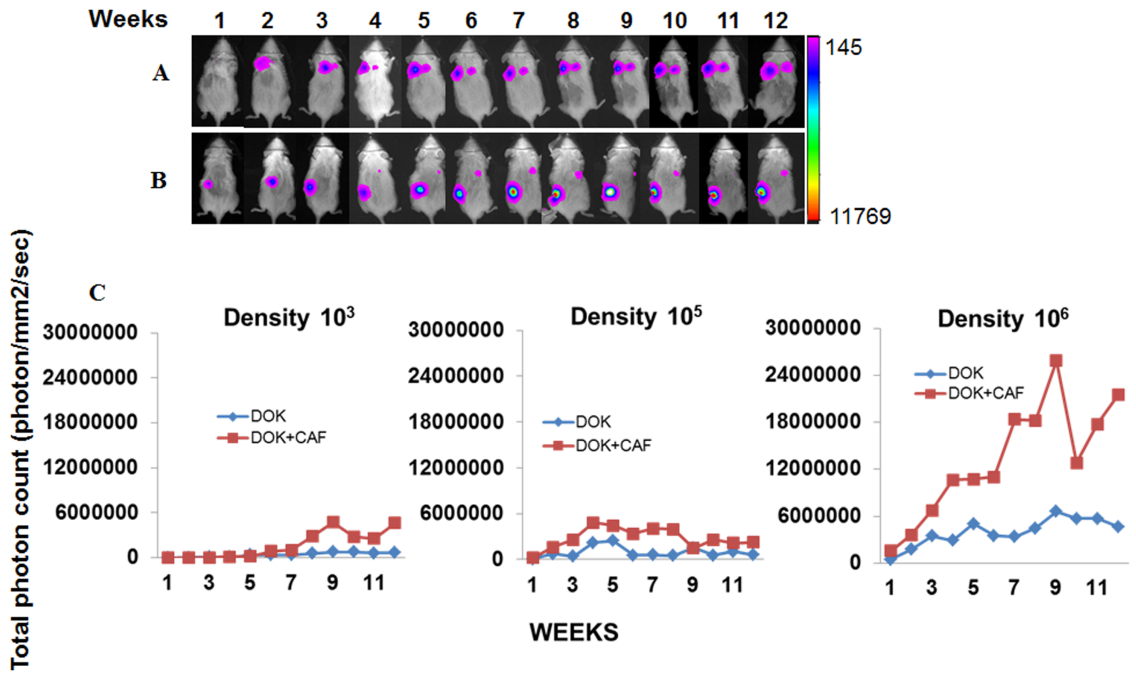

FIGURE 6. (A) Bioluminescence images of a representative mouse carrying a scaffold with a low density (1×10^3) in the upper right back and high density (1×10^6) of early neoplastic oral keratinocyte luciferase-transduced (DOK^{Luc}) alone in the upper left back. (B) Developing tumors with bioluminescence imaging of mice carrying low density (upper right) and high density (lower left) of DOK^{Luc} cocultured with (1×10^5) carcinoma-associated fibroblasts (CAFs). (C) Total photon count from in vivo imaging using DOK^{Luc} at different densities showed significantly higher bioluminescent intensity of scaffolds xenotransplanted with DOK^{Luc} + CAFs than of DOK^{Luc} alone throughout 12 weeks of imaging (10^6: $p < .001$; 10^5: $p < .001$; and 10^3: $p = .017$; $n = 6$).

xenotransplanted with DOK^{Luc} + CAFs than of DOK^{Luc} alone at all densities, just above the threshold 1 week after xenotransplantation and throughout the 12 weeks of in vivo imaging (10^6: $p < .001$; 10^5: $p < .001$; 10^3: $p = .017$; Figure 6C). In the scaffolds xenotransplanted with DOK^{Luc} alone, no tumors were formed outside the scaffolds and the bioluminescence signal stayed within the same range throughout the 12 weeks of imaging (Figure 6A). In contrast, the bioluminescence intensity of scaffolds cocultured with CAFs increased with time (Figure 6B), indicating an increase in tumor growth over time, and this was confirmed by histology. After 12 weeks, histological analysis of xenotransplants of scaffolds with DOK^{Luc} cells alone showed the presence of few atypical epithelial cells, limited to the scaffold area (Figures 7A, 7B, 7F, and 7G). Around the remnants of the scaffolds, scattered giant cells of mouse origin were observed (Figure 7K, blue arrow). The origin of the epithelial cells was confirmed by immunostaining using an antibody against human p53, recognizing only p53 mutated human cells, DOK. In contrast, the histology of xenografts of DOK^{Luc} + CAFs scaffolds showed squamous epithelial tumor nests (confirmed by p53 positive staining; Figures 7C, 7D, 7I, and 7J), with many of the islands retaining differentiation and containing keratin pearls, growing within and outside the scaffold area, invading the surrounding connective tissue and musculature, thus displaying the characteristic hallmarks of head and neck carcinoma. Few fibroblasts were observed in the xenotransplants even after 12 weeks of growth in vivo in mice (Figure 7K, black arrow). Figure 7E shows the pronounced macroscopic differences observed during harvesting of the scaffolds.

DISCUSSION

This study describes the development of a noninvasive, in vivo model for testing the tumorigenic potential of various microenvironmental cues, including scaffolds intended for use in tissue engineering. Numerous studies[34] support the concept that carcinogenesis, including head and neck cancer, is a multistep process involving a premalignant phase of long-term accumulated chromosomal alterations.[35] The use of normal cells in tumor models is time-consuming, if not irrelevant, because it is well-known that the transformation of human cells is a long process, involving at least 5 to 7 mutagenic events, which are difficult to achieve in an experimental setting.[20,36] For the present model, the DOK cell line, exhibiting early neoplastic epithelial dysplastic features was selected as a "screening sensor."[23] To facilitate the noninvasive visualization of these cells after xenotransplantation, they were transduced with luciferase gene, successfully generating a new cell line, DOK^{Luc}. The in vitro growth and behavioral characteristics of the transfected cells were comparable to those of the parent cells. To evaluate their behavior in vivo, both cell lines (DOK^{WT} and DOK^{Luc}) were xenotransplanted alone at low and high densities, both orthotopically, in the tongue, and ectopically, on the back of NSG mice. With a single exception for the tumor size when injected in the tongue at high density, DOK^{WT} and DOK^{Luc} showed a comparable in vivo behavior as well.

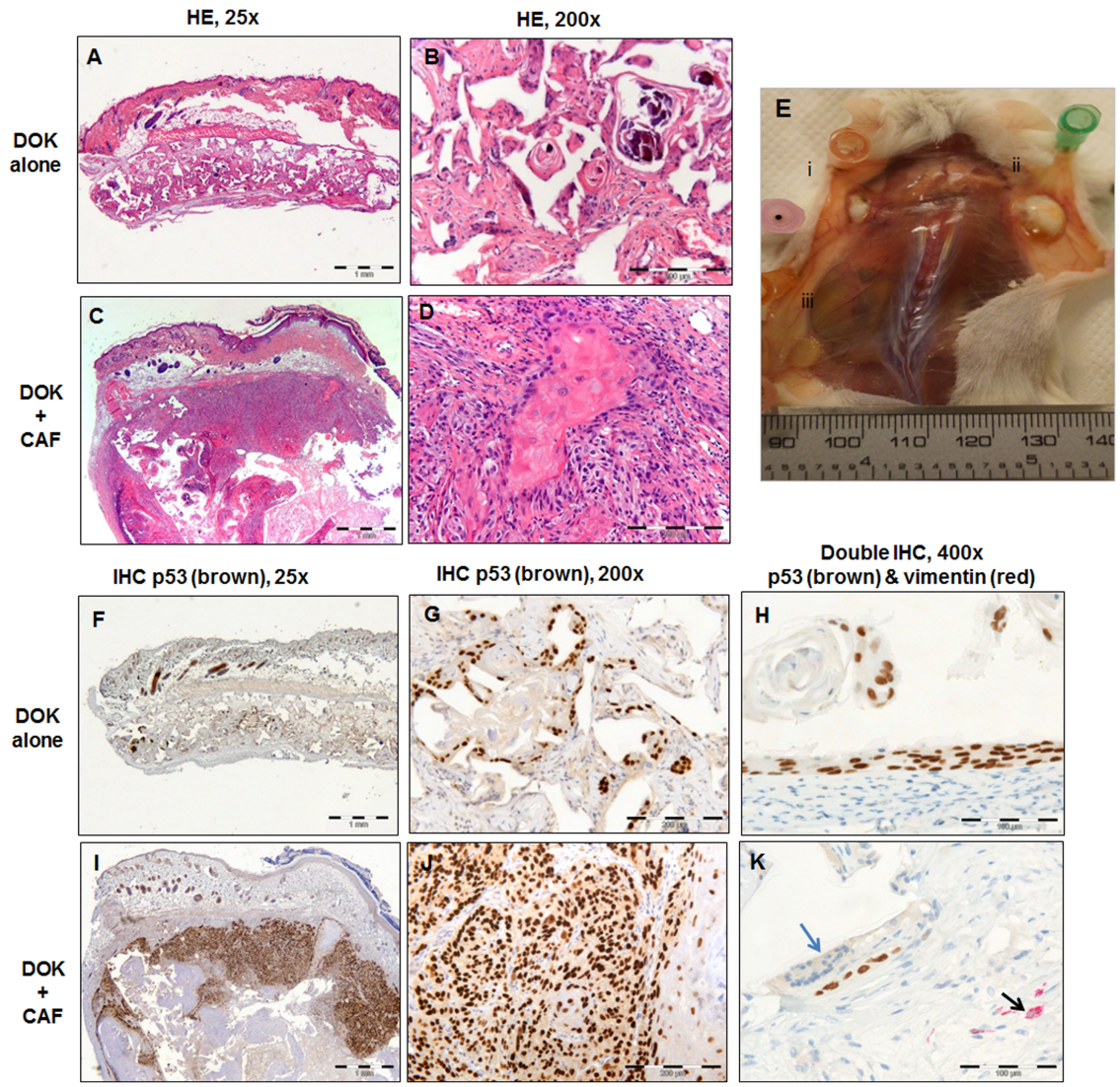

FIGURE 7. (A–D) Hematoxylin-eosin staining showing histology of early neoplastic oral keratinocyte luciferase-transduced (DOK^{Luc}) and DOK^{Luc} + carcinoma-associated fibroblasts (CAFs) xenografts respectively. (E) Dissection of a mouse after 12 weeks showing implanted scaffolds with: (1) 10^5 DOK^{Luc} cells alone; (2) 10^5 DOK^{Luc} cocultured with 10^5 CAF; and (3) empty scaffold. (F and G) Human p53 immunohistochemistry (IHC) showing the presence of few surviving human p53 mutated transformed epithelial cells in a scaffold xenotransplanted with DOK^{Luc} alone. (I and J) Human p53 immunohistochemistry showing islands of atypical epithelial cells within and outside the scaffold in DOK^{Luc} + CAFs xenografts (original magnification ×25 and ×200). Scale bar = 1 mm and 200 μm, respectively. (H and K) Double staining for human vimentin (red cytoplasmic stain) and human p53 (brown nuclear stain). (K) Positive vimentin stained human fibroblasts present after 12 weeks in DOK^{Luc} + CAFs xenografts (black arrow). The giant cells are negative for both human markers (blue arrow). Scale bar 100 μm (original magnification ×400).

This indicates that the DOK cell line retained a high degree of stability after transfection, although it carried a complex karyotype and multiple mutations, including p53 mutations. In accordance with previous oral carcinogenesis animal studies, the incidence and size of subcutaneous tumors in the present study was lower than those of tongue tumors.[16] This could be related to a greater stimulation of lymphangiogenesis in the tongue area[16] or simply because of the fact that orthotopic models allow cells to grow better in their original environment.

When DOK^{WT} cells were co-inoculated with CAFs in the tongue, the incidence of tumor formation increased by more than 40% compared with tumors formed by DOK^{WT} alone. This further highlights the important role of the microenvironmental cues in tumor initiation and early growth, supporting previous studies.[37,38] The tumor detected by manual measurements formed by DOK^{WT} was proven later on, histologically, to contain mainly remnants of matrigel, which might have given the mass that could be measurable by the caliper, and only few islands of nonproliferative DOK cells. This illustrates one of the drawbacks of the manual measurements that can be avoided by the use of other methods, such as bioluminescence.

In this study, bioluminescence detected more than 50% of the total number of tumors formed in the tongue by DOK^{Luc} from the first week; much earlier than tumor detection with caliper measurements. In the skin tumors,

6 of 7 were visible by bioluminescence from the first week. One of the tumors was from low density inoculations, which were too small for detection by manual measurements, but it was later confirmed histologically. The total number of tumors detected by bioluminescence was significantly greater than manual detection ($p = .043$), and in concordance with the histological findings, indicating higher sensitivity for early detection using the bioluminescence method.

The measurements from the last timepoint of tumor growth assessment period showed higher bioluminescence signals from tumors with CAF15_23 than those with CAF15_13; this difference was not detected by the manual measurements. Histological evaluation confirmed statistically bigger tumors formed by DOK^{Luc} co-injected with the CAF15_23, a difference that was not indicated by the manual measurements. This brings further indications for the greater sensitivity of the bioluminescence method compared to the manual method that might carry subjective evaluations (eg, inflammation, tongue pull, position of the mouse, and lesion margins).

Degradable copolymer scaffolds were used to further optimize and validate the model for use in screening tests for tumorigenesis of various microenvironmental cues from biomaterials. The manual monitoring of tumors at early stages was impossible because the tumors initially developed within the scaffold. However, this was not an impediment for bioluminescence. The correlation between bioluminescence signals and the golden standard method of histological examination was higher, confirming the method is more sensitive than manual measurements. Therefore, bioluminescence was further used solely to monitor the scaffolds when developing the model.

A challenge for using the bioluminescence method would be monitoring of bigger tumors. We monitored a drop in intensity for a tumor developed from very high seeding density of DOK^{Luc} + CAFs xenografts (1×10^6). We interpreted that to be an underestimation of the real bioluminescence signal from the cells because that tumor was later found to be cystic. Cystic content or necrosis that can occur in large or late stage tumors might reduce the production of light because of decreased proliferation or hypoxia.[27,39] Therefore, we recommend inoculating fewer cells per area of scaffold in order to circumvent these limitations and monitor tumor formation for longer period of times, as required in carcinogenesis studies. Although the use of such immunodeficient models greatly aids the development of "humanized" models of cancer using biomaterials,[25] it does come with the caveat of no innate host immunity. Whereas this limitation prevents the current study of role of the immune system in tumor prevention in such models or the use of immunotherapeutic interventions, steps have been made to circumvent such constraints. Recent efforts have demonstrated that introduction of distinct human immune components are possible in mice xenografted with cancer cell lines,[40] suggesting that further evolution of the NSG mice system may yet render models to study human immune reactions in cancer.

Our model provides an abridged alternative to the years spent in rodent models to get tumors from biomaterials implanted solely in animals and foreign body tumorigenesis has several stages, with specific sequences of preneoplastic characteristics.[12,41] The processing time is reduced because of the ability of screening several animals simultaneously, which makes it cheaper compared to other high throughput imaging methods used in the field, such as MRI.

CONCLUSIONS

The model generated and validated in this study is a sensitive and reliable model for monitoring microenvironmentally induced carcinogenesis providing early, consistent surveillance of tumor development associated with implantation of scaffolds for tissue engineering.

Acknowledgments

The authors thank Dr. Joan Bevenius–Carrick, Dr. Andrew Davis, and Prof. Mustafa Nur Elhuda for English revision and constructive criticism of the manuscript. We are grateful to Tereza Osdal (University of Bergen) for assistance with cell transduction, Gunnvor Øijordsbakken (Gade Laboratory for Pathology) for support with histology, and Mihaela Popa (Kin*N* Therapeutics AS, Bergen) for bioluminescence imaging training. The bioluminescence imaging was performed at the Molecular Imaging Centre (MIC), University of Bergen.

REFERENCES

1. De Wever O, Mareel M. Role of tissue stroma in cancer cell invasion. *J Pathol* 2003;200:429–447.
2. Kalluri R, Zeisberg M. Fibroblasts in cancer. *Nat Rev Cancer* 2006;6:392–401.
3. Mantovani A, Allavena P, Sica A, Balkwill F. Cancer-related inflammation. *Nature* 2008;454:436–444.
4. Anderson JM, Rodriguez A, Chang DT. Foreign body reaction to biomaterials. *Semin Immunol* 2008;20:86–100.
5. Nakamura T, Shimizu Y, Okumura N, Matsui T, Hyon SH, Shimamoto T. Tumorigenicity of poly-L-lactide (PLLA) plates compared with medical-grade polyethylene. *J Biomed Mater Res* 1994;28:17–25.
6. Nakamura T, Shimizu Y, Takimoto Y, et al. Biodegradation and tumorigenicity of implanted plates made from a copolymer of epsilon-caprolactone and L-lactide in rat. *J Biomed Mater Res* 1998;42:475–484.
7. Kirkpatrick CJ, Alves A, Köhler H, et al. Biomaterial-induced sarcoma: a novel model to study preneoplastic change. *Am J Pathol* 2000;156:1455–1467.
8. Idris SB, Dånmark S, Finne–Wistrand A, et al. Biocompatibility of polyester scaffolds with fibroblasts and osteoblast-like cells for bone tissue engineering. *J Bioact Compat Polym* 2010;25:567–583.
9. ISO/EN ID. Biological evaluation of medical devices-part 5. Test for cytotoxicity: in vitro methods. Geneva, Switzerland: International Organisation of Standardisation; 1992.
10. Kato S, Akagi T, Sugimura K, Kishida A, Akashi M. Evaluation of biological responses to polymeric biomaterials by RT-PCR analysis IV: study of c-myc, c-fos and p53 mRNA expression. *Biomaterials* 2000;21:521–527.
11. Carraway J, Ghosh C. The challenge to global acceptance of part 3 of ISO 10993. *Med Device Technol* 2006;17:16–18.
12. Takanashi S, Hara K, Aoki K, et al. Carcinogenicity evaluation for the application of carbon nanotubes as biomaterials in rasH2 mice. *Sci Rep* 2012;2:498.
13. Cohen SM. Human carcinogenic risk evaluation: an alternative approach to the two-year rodent bioassay. *Toxicol Sci* 2004;80:225–229.
14. Ward JM. The two-year rodent carcinogenesis bioassay – Will it survive? *J Toxicol Pathol* 2007;20:13–19.
15. Ahmed SU, Zair M, Chen K, et al. Generation of subcutaneous and intrahepatic human hepatocellular carcinoma xenografts in immunodeficient mice. *J Vis Exp* 2013;79:e50544.
16. Hadler–Olsen E, Wetting HL, Rikardsen O, et al. Stromal impact on tumor growth and lymphangiogenesis in human carcinoma xenografts. *Virchows Arch* 2010;457:677–692.
17. Ruggeri BA, Camp F, Miknyoczki S. Animal models of disease: preclinical animal models of cancer and their applications and utility in drug discovery. *Biochem Pharmacol* 2013;87:150–161.
18. Sano D, Myers JN. Xenograft models of head and neck cancers. *Head Neck Oncol* 2009;1:32.

19. Bibby MC. Orthotopic models of cancer for preclinical drug evaluation: advantages and disadvantages. *Eur J Cancer* 2004;40:852–857.
20. Debnath J, Brugge JS. Modelling glandular epithelial cancers in three-dimensional cultures. *Nat Rev Cancer* 2005;5:675–688.
21. Warnakulasuriya S. Global epidemiology of oral and oropharyngeal cancer. *Oral Oncol* 2009;45:309–316.
22. Yang K, Zhao N, Zhao D, Chen D, Li Y. The drug efficacy and adverse reactions in a mouse model of oral squamous cell carcinoma treated with oxaliplatin at different time points during a day. *Drug Des Devel Ther* 2013;7:511–517.
23. Chang SE, Foster S, Betts D, Marnock WE. DOK, a cell line established from human dysplastic oral mucosa, shows a partially transformed non-malignant phenotype. *Int J Cancer* 1992;52:896–902.
24. Khemthongcharoen N, Jolivot R, Rattanavarin S, Piyawattanametha W. Advances in imaging probes and optical microendoscopic imaging techniques for early in vivo cancer assessment. *Adv Drug Deliv Rev* 2013;74:53–74.
25. Lee J, Li M, Milwid J, et al. Implantable microenvironments to attract hematopoietic stem/cancer cells. *Natl Acad Sci U S A* 2012;109:19638–19643.
26. McCormack E, Silden E, West RM, et al. Nitroreductase, a near-infrared reporter platform for in vivo time-domain optical imaging of metastatic cancer. *Cancer Res* 2013;73:1276–1286.
27. Jarzabek MA, Huszthy PC, Skaftnesmo KO, et al. In vivo bioluminescence imaging validation of a human biopsy-derived orthotopic mouse model of glioblastoma multiforme. *Mol Imaging* 2013;12:161–172.
28. Kotopoulis S, Delalande A, Popa M, et al. Sonoporation-enhanced chemotherapy significantly reduces primary tumour burden in an orthotopic pancreatic cancer xenograft. *Mol Imaging Biol* 2014;16:53–62.
29. Zinn KR, Chaudhuri TR, Szafran AA, et al. Noninvasive bioluminescence imaging in small animals. *ILAR J* 2008;49:103–115.
30. Pinsky MS, Song W, Dong Z, et al. Activation of iCaspase-9 in neovessels inhibits oral tumor progression. *J Dent Res* 2006;85:436–441.
31. Warner KA, Miyazawa M, Cordeiro MM, et al. Endothelial cells enhance tumor cell invasion through a crosstalk mediated by CXC chemokine signaling. *Neoplasia* 2008;10:131–139.
32. Dånmark S, Finne–Wistrand A, Wendel M, Arvidson K, Albertsson A-C, Mustafa K. Osteogenic differentiation by rat bone marrow stromal cells on customized biodegradable polymer scaffolds. *Bioact Compat Polym* 2010;25:207–223.
33. McCormack E, Haaland I, Venås G, et al. Synergistic induction of p53 mediated apoptosis by valproic acid and nutlin-3 in acute myeloid leukemia. *Leukemia* 2012;26:910–917.
34. Hanahan D, Weinberg RA. Hallmarks of cancer: the next generation. *Cell* 2011;144:646–674.
35. Vineis P, Schatzkin A, Potter JD. Models of carcinogenesis: an overview. *Carcinogenesis* 2010;31:1703–1709.
36. Leemans CR, Braakhuis BJ, Brakenhoff RH. The molecular biology of head and neck cancer. *Nat Rev Cancer* 2011;11:9–22.
37. Clark AK, Taubenberger AV, Taylor RA, et al. A bioengineered microenvironment to quantitatively measure the tumorigenic properties of cancer-associated fibroblasts in human prostate cancer. *Biomaterials* 2013;34:4777–4785.
38. Costea DE, Hills A, Osman AH, et al. Identification of two distinct carcinoma-associated fibroblast subtypes with differential tumor-promoting abilities in oral squamous cell carcinoma. *Cancer Res* 2013;73:3888–3901.
39. Black PC, Shetty A, Brown GA, et al. Validating bladder cancer xenograft bioluminescence with magnetic resonance imaging: the significance of hypoxia and necrosis. *BJU Int* 2010;106:1799–1804.
40. McCormack E, Adams KJ, Hassan NJ, et al. Bi-specific TCR-anti CD3 redirected T-cell targeting of NY-ESO-1- and LAGE-1-positive tumors. *Cancer Immunol Immunother* 2013;62:773–785.
41. Moizhess TG. Carcinogenesis induced by foreign bodies. *Biochemistry (Mosc)* 2008;73:763–775.